ACS APPLIED MATERIALS & INTERFACES

Research Article

www.acsami.org

High-Temperature Stability and Saturation Magnetization of Superparamagnetic Nickel Nanoparticles in Microporous Polysilazane-Derived Ceramics and their Gas Permeation Properties

Mahdi Seifollahi Bazarjani,*[,†,‡] Mathis M. Müller,[†] Hans-Joachim Kleebe,[†] Yvonne Jüttke,[§] Ingolf Voigt,[§] Mehrdad Baghaie Yazdi,[†] Lambert Alff,[†] Ralf Riedel,[†] and Aleksander Gurlo[†,#]

[†]Fachbereich Material-und Geowissenschaften, Technische Universität Darmstadt, Jovanka Bontschits Strasse 2, D-64287 Darmstadt, Germany

[§]Fraunhofer Institute for Ceramic Technologies and Systems, Michael-Faraday Strasse 1, D-07629 Hermsdorf, Germany

Supporting Information

ABSTRACT: Superparamagnetic Ni nanoparticles with diameters of about 3 nm are formed in situ at room temperature in a polysilazane matrix, forming Ni/polysilazane nanocomposite, in the reaction between a polysilazane and *trans*-bis(aceto-*k*O)bis(2-aminoethanol-k^2N,O)nickel(II). The thermolysis of the Ni/polysilazane nanocomposite at 700 °C in an argon atmosphere results in a microporous superparamagnetic Ni/silicon oxycarbonitride (Ni/SiCNO) ceramic nanocomposite. The growth of Ni nanoparticles in Ni/SiCNO ceramic nanocomposite is totally suppressed even after thermolysis at 700 °C, as confirmed by HRTEM and SQUID characterizations. The analysis of saturation magnetization of Ni nanoparticles in Ni/polysilazane and Ni/SiCNO nanocomposites indicates that the saturation magnetization of Ni nanoparticles is higher than expected values and infers that the surfaces of Ni nanoparticles are not oxidized. The microporous superparamagnetic Ni/SiCNO nanocomposite is shaped as a free-standing monolith and foam. In addition, Ni/SiCNO membranes are fabricated by the dip-coating of a tubular alumina substrate in a dispersion of Ni/polysilazane in THF followed by a thermolysis at 700 °C under an argon atmosphere. The gas separation performance of Ni/SiCNO membranes at 25 and 300 °C is assessed by the single gas permeance (pressure rise technique) using He, H_2, CO_2, N_2, CH_4, n-propene, n-propane, n-butene, n-butane, and SF_6 as probe molecules. After hydrothermal treatment, the higher increase in the hydrogen permeance compared to the permeance of other gases as a function of temperature indicates that the hydrogen affinity of Ni nanoparticles influences the transport of hydrogen in the Ni/SiCNO membrane and Ni nanoparticles stabilize the structure against hydrothermal corrosion.

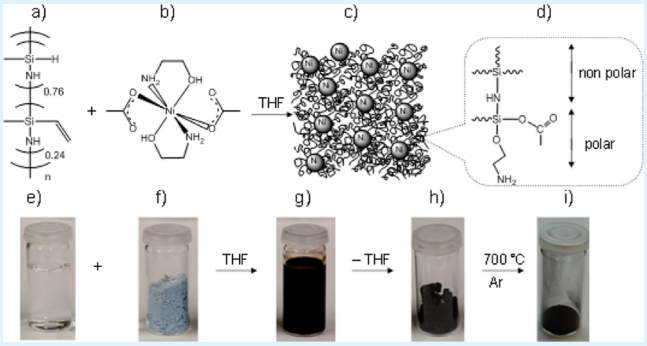

KEYWORDS: *Ni/polysilazane, Ni/SiCNO, superparamagnetic, permeance, membrane*

INTRODUCTION

Microporous silica (SiO_2) is widely studied as membranes for hydrogen separation and purification, which are typically synthesized by sol–gel method[1,2] and chemical vapor deposition (CVD).[3−6] However, the application of SiO_2 membranes is limited because of the degradation of microporous structure under hydrothermal conditions.[7] Si-containing ceramics derived from preceramic polymers (so-called polymer-derived ceramics, PDCs) have gained particular attention in recent years. They have been applied as novel materials for environmental and energy applications,[8−13] including gas separation.[12,14,15] However, PDCs are also characterized by limited hydrothermal stability which hinders their application for gas separation.

Here, we apply a novel synthetic approach to in situ form Ni nanoparticles in a polysilazane which after thermolysis leads to the formation of suitable Ni/silicon oxycarbonitride (SiCNO) nanocomposites for gas separation.

Our interest for the application of Ni nanoparticles in SiCNO ceramics originates from the fact that metal (e.g., Ni)[16−18] and metal oxide (e.g., Co_3O_4)[2] nanoparticles have been used to enhance the stability of silica membranes under hydrothermal conditions.[2,16,17,19−21] Here, we explore the possibility to extend the application of well-dispersed Ni nanoparticles in a SiCNO ceramic for the preparation of membranes which are stable under hydrothermal conditions.

The dispersion of metallic nanoparticles in PDCs is usually achieved by mixing preceramic polymers with proper additives followed by thermolysis under a controlled atmosphere. For

Received: March 28, 2014
Accepted: July 11, 2014
Published: July 11, 2014

example, M/SiCNO (M = Ni, Fe) ceramics are synthesized at ~700−1000 °C under an inert atmosphere from polysilazanes mixed with Fe/Fe_3O_4 and Ni powders.[22] The drawback of this approach is the nonuniform dispersion and agglomeration of nanoparticles. The uniform dispersion of nanoparticles in the PDC nanocomposites is achieved by the thermal decomposition of (i) metallopolymers, and (ii) polymers reacted with organometallic compounds.[23]

Among different methods used for the synthesis of Ni nanoparticles, solution phase synthesis has been most widely applied; because of simplicity, flexibility and better control over size as well as the distribution of Ni nanoparticles.[24−26] However, a major problem in the solution phase synthesis is the agglomeration and growth of nanoparticles, which is avoided by using surfactants and block copolymers.[24,27] In addition, the thermal treatment of nanoparticles at high temperatures destroys the organic shells leading to the growth of nanoparticles and their agglomeration.[28]

Here, we apply Superconducting QUantum Interference Device (SQUID) to characterize the size of superparamagnetic Ni nanoparticles encapsulated in a polysilazane and microporous SiCNO ceramic nanocomposite, Ni/polysilazane, and Ni/SiCNO, respectively. This analysis shows that the growth and agglomeration of very small Ni nanoparticles (2−3 nm) are totally suppressed even at temperatures as high as 700 °C under an argon (Ar) atmosphere. Further analysis of the saturation magnetization (Ms) of Ni nanoparticles based on a core−shell model indicates that the developed synthetic strategy for the preparation of Ni/polysilazane and Ni/SiCNO nanocomposite preserves the surfaces of Ni nanoparticles against oxidation. This is important, as the Ni nanoparticles that are well-preserved in the ceramic matrix have H_2 affinity and increase the H_2 permeance of as-prepared Ni/SiCNO membrane specifically after hydrothermal treatment.

EXPERIMENTAL METHODS

Synthesis of Ni/Polysilazane and Ni/SiCNO Nanocomposites. We have recently reported the in situ formation of Ni nanoparticles at room temperature, during the course of reaction between the poly(vinylmethyl)-*co*-poly(methylhydro)silazane (polysilazane hereafter, Figure 1a, e) and trans-bis(acetato-*k*O)bis(2-aminoethanol-k^2N,O)nickel(II) (Ni(II)-complex hereafter, Figure 1b, f).[29,30]

This reaction results in a stable dispersion of Ni nanoparticles in THF (Figure 1g). After removing THF under vacuum, a superparamagentic material, containing well-dispersed Ni nanoparticles is obtained. The in situ formation and stabilization of the Ni nanoparticles are achieved by (i) the reducing silane groups, and (ii) in situ formed amphiphilic molecules, respectively.[29]

The reaction between the polysilazane and Ni(ii)-complex causes the release of some of silazane bonds in the form of ammonia.[29] The Ni/polysilazane sample used here is the result of the reaction between 40 wt % Ni(II)-complex and the polysilazane. The elemental composition of the thermolysis product of this Ni/polysilazane sample at 700 °C (the details of thermolysis profile are mentioned in the next section) indicates, Si, C, N, O, and H content of 33.15, 20.10, 3.32, 28.43, and 2.16 wt %, respectively, corresponding to empirical formula of $0.13Ni/Si_1C_{1.41}N_{0.2}O_{1.5}H_{1.83}$.[29]

Ceramic Monolith, Foam, and Membrane Preparation. The Ni/polysilazane was subjected to the variety of different shaping techniques and thermolyzed based on the following thermolysis profile to fabricate Ni/SiCNO ceramic monolith, foam, and membrane.

Thermolysis Profile Applied for the Synthesis of Ni/SiCNO Monolith, Foam, and Membrane. The specimens were thermolyzed under Ar flow (75 cm^3 min^{-1}) by the following thermolysis profile:

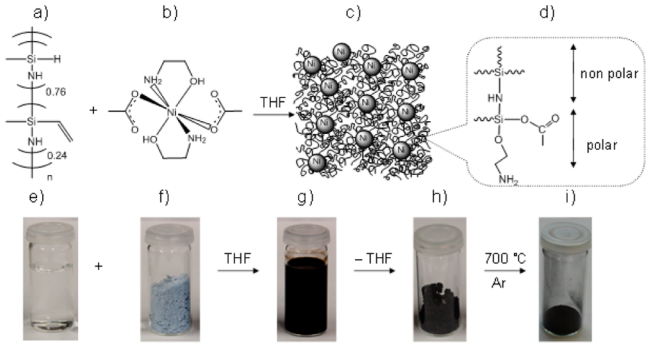

Figure 1. (a, e) Polysilazane reacted with (b, f) 40 wt % Ni(II)-complex to form (c, g, h) superparamagnetic Ni/polysilazane nanocomposite. (d) Nucleophilic substitution of ethanolamine and acetate groups at the Si centers in the polysilazane replaces silazane linkages (-Si-NH-Si-) with aminoethoxysilyl ($NH_2CH_2CH_2OSi$-) and acetoxysilyl (CH_3COOSi-) groups forming amphiphilic polysilazane molecules. (g) Ni nanoparticles are encapsulated by amphiphilic polysilazane molecules and are sterically stabilized in solution. (g) Dispersion of Ni/polysilazane in THF results in (h) a superparamagnetic elastomer, which after thermolysis at 700 °C transforms into (i) a superparamagnetic Ni/SiCNO nanocomposite.

heated from room temperature with a rate of 100 °C h^{-1} to 200 °C, hold for 4 h at 200 °C, further heated to 300 °C with a rate of 50 °C h^{-1}, hold for 10 h at 300 °C, further heated to 400 °C with a rate of 50 °C h^{-1}, hold for 10 h at 400 °C, further heated to 500 °C with a rate of 50 °C h^{-1}, hold for 10 h at 500 °C, further heated to 700 °C with a rate of 100 °C h^{-1}, and finally cooled to room temperature with a rate of 50 °C h^{-1}.

Green Body and Ceramic Monolith Preparation. The Ni/polysilazane nanocomposite was heated under Ar flow (75 cm^3 min^{-1}) to 235 °C with a rate of 100 °C h^{-1}, hold for 3 h, and cooled down to room temperature with a rate of 50 °C h^{-1}. Then the obtained chunk was well-milled in a glovebox to obtain a fine powder. The latter powder was warm pressed at 200 °C and 50 kN for 2 h to make the green body. The as-prepared green body was thermolyzed using the above-mentioned thermolysis profile to obtain ceramic monolith.

Ceramic Foam Preparation. Using Schlenk techniques, a cross-linked polyurethane foam template was immersed in a 5 wt % dispersion of Ni/polysilazane nanocomposite in THF for 5 min, and then it was taken out and dried for 10 min under Ar flow at room temperature. This procedure was repeated for 5 times. Afterward, the foam template coated with the Ni/polysilazane precursor was thermolyzed on the basis of the above-mentioned thermolysis profile to obtain the ceramic foam.

Deposition of Membranes. The alumina tubular substrate coated with a graded porous structure was supplied from Fraunhofer IKTS (Hermsdorf). In a glovebox, the inner surface of a γ-alumina coated tubular substrate was dip coated in the 5 wt % dispersion of Ni/polysilazane nanocomposite in THF for 1 min, and then it was dried for 4 h at room temperature. The Ni/polysilazane coating was thermolyzed using the above-mentioned thermolysis profile to obtain the ceramic membrane. The whole procedure was repeated 3 times.

Hydrothermal Treatment. The hydrothermal treatment of membranes was performed at 180 °C and 50 bar for 24 h, using H_2O and air mixtures (50/50).

Characterization. The Ni content was determined at the Mikroanalytisches Labor Pascher (Remagen, Bendorf-Germany), applying the Coupled Plasma Atomic Emission Spectroscopy (Thermo Instruments, iCAP 6500) and Elementanalyzer (Pascher).

X-ray powder patterns were obtained by a STOE X-ray diffractometer with Ge (111) monochromator and Mo K_α radiation.

High resolution transmission electron microscopy (HRTEM) was performed at a FEI CM20STEM instrument operated at 200 kV (FEI, Eindhoven, The Netherlands). For Ni/SiCNO nanocomposite,

powder was dispersed in ethanol and deposed on a carbon coated Cu-grid (Plano, Germany). For the Ni/polysilazane nanocomposite, a droplet from the Ni/polysilazane dispersion in THF was deposed on the carbon coated Cu-grid (Plano, Germany). The latter samples were lightly carbon-coated to minimize charging under incident electron beam.

Dynamic light scattering (DLS) was performed on diluted (1/20) Ni/polysilazane nanocomposite dispersed in THF using Nano ZS (Malvern Instruments) with a laser wavelength of 532 nm capable of measuring particle size range of 0.6 nm to 2 μm. The size distribution of the nanoparticles was averaged from five reproducible measurements.

Magnetization was measured by a Magnetic Property Measurement System (MPMS, Quantum Design), using a Superconducting QUantum Interference Device (SQUID) in the temperature range of 2 to 300 K with an applied field of 500 Oe. Furthermore, the magnetization as a function of applied field (from −15 000 to 15 000 Oe) was recorded at 300 K.

Infrared spectra were recorded with a Bruker Vertex 70 FT-IR spectrometer (Bruker, USA) in transmission geometry, using KBr pellets.

Gas Permeance Characterizations.[31] The single gas permeance of the membranes was measured applying the pressure rise technique in a dead end cell using gases with different kinetic diameters: He (0.26 nm), H_2 (0.289 nm), CO_2 (0.33 nm), N_2 (0.36 nm), CH_4 (0.38 nm), n-propene (0.44 nm), n-propane (0.43 nm), n-butene (0.45 nm), n-butane (0.47 nm), and SF_6 (0.51 nm) at 25 and 300 °C. After evacuating feed- and permeate-site and tempering the module and gas pipes at the specific temperatures the gas streamed into the feed room and pressure increase on permeate site was measured. From linear part of the pressure increase mass flow was determined. Ideal permselectivity was calculated as the ratio of the permeance of a gas to that of H_2.

Pore volume and surface area analysis of the ceramic powders were carried out according to Brunauer−Emmett−Teller (BET) method by N_2 sorption isothermal analysis at −196 °C (Model Autosorb-1, Quantachrome Instruments, USA) after powdered samples were outgassed at 150 °C for 24 h. The microporosity analyses of ceramic powders were done by adsorbed layer thickness method (t-method).

RESULTS AND DISCUSSION

High-Temperature Stability of Ni Nanoparticles in Silicon Oxycarbonitride Ceramics. We demonstrate quantitatively here that the encapsulation of Ni nanoparticles in the polymeric matrix prevents their growth and agglomeration, resulting in their unique stability even after polymer-to-ceramic transformation at a high temperature under an inert atmosphere.

Figure 2a displays the temperature dependence of the zero-field-cooled (ZFC) magnetization of the Ni/polysilazane and Ni/SiCNO nanocomposites measured at 500 Oe.

Neither a maximum in the temperature-dependent magnetization (Figure 2a), nor a hysteresis loop and remnant magnetization in the field-dependent magnetization (Figure 2b) is observed, indicating Ni nanoparticles in so-called superparamagnetic state.

The extremely reduced blocking temperature, which is below 2−3 K in the Ni/polysilazane and Ni/SiCNO nanocomposites (Figure 2a) points out that the size of the Ni nanoparticles is well-below 10 nm.[32]

In the next step, we calculate the magnetic moment and size of the Ni nanoparticles dispersed in the polysilazane and SiCNO ceramics, by a reported procedure.[33−35]

In a superparamagnetic material with the thermal energy larger than the magnetic anisotropy energy, the standard Langevin function describes the magnetization M as follows[36−38]

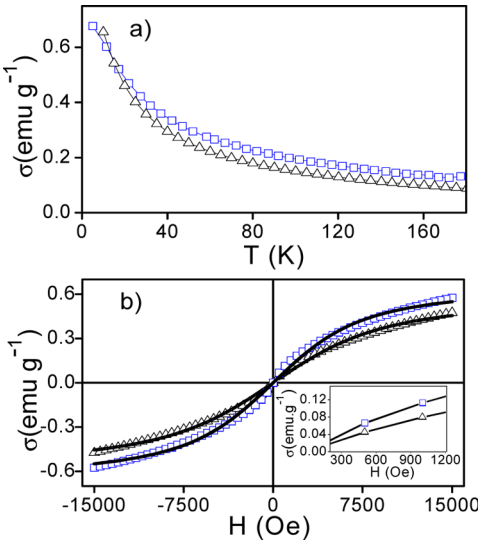

Figure 2. Temperature-dependent magnetization at 500 Oe with (a) zero-field-cooling and (b) field-dependent magnetization at 300 K with a close-up in the inset of Ni/polysilazane (Δ) and Ni/SiCNO (□). The measured data (points) in b are fitted with the Langevin function (black lines, see eq 1 and text for details).

$$\frac{M}{M_s} = \coth\left(\frac{\mu H}{K_b T}\right) - \left(\frac{K_b T}{\mu H}\right) \quad (1)$$

where M_s refers to saturation magnetization, μ is average magnetic moment of a particle, k_b is the Boltzmann constant, T is temperature, and H is applied magnetic field.

After fitting the field-dependent magnetization of the Ni/polysilazane and Ni/SiCNO with the Langevin function (eq 1, black lines in Figure 2b), we obtain the saturation magnetization and the average magnetic moment for the Ni/polysilazane and Ni/SiCNO nanocomposites, M_s = 0.602 ± 0.008 emu g^{-1}/μ = 1209 ± 29 μ_B and M_s = 0.680 ± 0.008 emu g^{-1}/μ = 1516 ± 39 μ_B, respectively (μ_B is the Bohr magneton).

The average magnetic moment μ of a Ni nanoparticle, containing "N" nickel atoms and each nickel atom with the magnetic moment μ_{Ni} is calculated by eq 2[36]

$$\mu = N\mu_{Ni} \quad (2)$$

When Ni nanoparticles contain more than ∼400 Ni atoms, μ_{Ni} becomes independent of the size and equals to that of the bulk value for Ni ($\mu_{Ni} \approx 0.57\ \mu_B$).[39]

The number of Ni atoms calculated by eq 2, fitted μ values and $\mu_{Ni} \approx 0.57\ \mu_B$ is 2121 ± 51 and 2659 ± 68 atoms in the Ni/polysilazane and Ni/SiCNO nanocomposites, respectively. The diameter (nm) of spherical Ni nanoparticles is calculated by eq 3

$$D = \sqrt[3]{\frac{6A_r N}{\pi \rho N_A}} = (0.275\sqrt[3]{N}) \quad (3)$$

where A_r and ρ are the relative atomic weight (58.70 g mol^{-1}) and density (8.91 g cm^{-3}) of Ni, respectively, and N_A is the Avogadro number (6.023 × 10^{23} mol^{-1}).

The diameter of the Ni nanoparticles from eq 3 is 3.5 ± 1 and 3.8 ± 1.1 nm in the Ni/polysilazane and Ni/SiCNO nanocomposites, respectively. These values show fair agreement with the diameter of Ni nanoparticles determined by HRTEM and DLS (Table 1).

Table 1. Average Ni Nanoparticles Diameter (nm) for Ni/Polysilazane and Ni/SiCNO Nanocomposites Determined by Complementary Methods: SQUID, HRTEM, and DLS

method	SQUID	HRTEM	DLS
Ni/polysilazane	3.5 ± 1.0	2.5 ± 0.5	3.0 ± 0.6
Ni/SiCNO	3.8 ± 1.1	3.0 ± 0.7	

Therefore, the uniform dispersion of nearly monodisperse Ni nanoparticles in the Ni/polysilazane and Ni/SiCNO nanocomposites is confirmed simultaneously by dynamic light scattering (DLS, Figure 3), high-resolution transmission

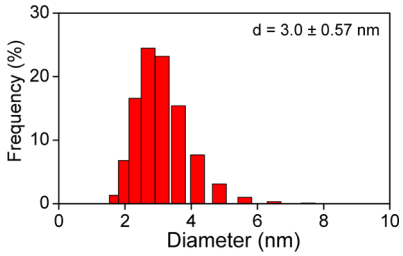

Figure 3. Size distribution of Ni nanoparticles determined by dynamic light scattering (DLS) from dispersion of Ni/polysilazane in THF (diluted; 1/20, average, and standard deviation are indicated).

electron microscopy (HRTEM, Figure S1 in the Supporting Information) and superconducting quantum interference device (SQUID, Figure 2) characterizations.

In the next section, we demonstrate that the Ni nanoparticles are so well-protected against oxidation in the modified polysilazane and SiCNO matrixes that their saturation magnetization values are much higher than expected ones.

Anomalous High Saturation Magnetization (M_s) of Ni Nanoparticles in Ni/SiCNO and Ni/Polysilazane Nanocomposites. The magnetic properties of materials at nanoscale are considerably different from those in bulk,[40] e.g., the significant reduction of magnetic moments is observed in nanoparticles.[40,41] This effect is explained by a core−shell model in which a shell of disordered spins significantly reduces the overall magnetic moment of a bulk-like magnetic core (Figure 4a).[33,41−48]

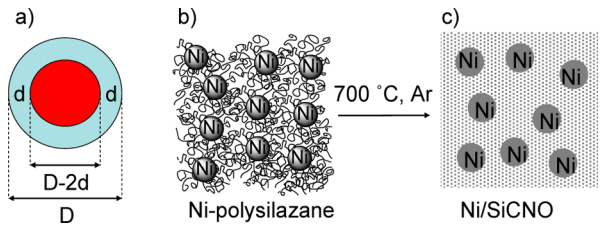

Figure 4. (a) Core−shell model describing (blue) disordered shell and (red) magnetic core, (b) scheme of microstructure of Ni/polysilazane, and (c) Ni/SiCNO nanocomposites with embedded Ni nanoparticles.

For example, the decrease of M_s in iron and maghemite nanoparticles with respect to that of the bulk is explained by oxide and disordered surface layers with a thickness of 1 and 1.5 nm, respectively.[41,44]

We investigate here an anomalous effect, i.e., an unusually higher than expected M_s of Ni nanoparticles in the Ni/polysilazane and Ni/SiCNO nanocomposites, when compared to that typically observed in the Ni nanoparticles of comparable size.

In the core-sell model the saturation magnetization (M_s) is proportional to the volume fraction of the magnetic core (M_{so}, eq 4)

$$M_s = M_{so}\left(\frac{D-2d}{D}\right)^3 \quad (4)$$

where D is the diameter of a nanoparticle and d is the thickness of a nanoparticle disordered shell (Figure 4). Therefore, as the particle size decreases the contribution of the disordered layer increases significantly approaching the limiting size value for total magnetic disorder.[41] For example, the maghemite nanoparticles with the diameter of about 3 nm and magnetic dead shell of 1.5 nm possess M_s close to zero.[40,41,44,45]

The constant thickness of this disordered surface layer in nanoparticles suggests the microscopic effects that are responsible for the decrease in M_s with the reduction in particle size are independent of the size of nanoparticles.

The first effect is the surface anisotropy that significantly reduces M_s at a given temperature.[42] Furthermore, the decrease in the coordination number of atoms on the surfaces of nanoparticles induces a weakening in the exchange interactions of the surface atoms with the surrounding ones; the results of that is an increased magnetic anisotropy compared to that in the core.[49] Another effect is related to the presence of impurities (e.g., the surface oxidation of ferromagnetic metallic nanoparticles) on the surfaces of nanoparticles that reduce the magnetic moment of nanoparticles. For example, in Ni nanoparticles a rough estimation shows that every oxygen atom destroys the contribution of one Ni atom to ferromagnetism and leads to a strong decrease in magnetization.[46]

Our specimens, i.e., the Ni/polysilazane and Ni/SiCNO nanocomposites, allow us to show the determining role of oxygen impurities on the M_s of Ni nanoparticles embedded in protective polysilazane polymer and silicon oxycarbonitrides ceramic matrixes.

Here, we apply the core−shell model to describe the dependence of M_s on the size of Ni nanoparticles from the literature and compare them with the M_s of Ni nanoparticles reported here. Table 2 and Figure 5 display this comparison.

Using eq 4, a fair fit is obtained for the previously published literature data (Figure 5a), which yields a magnetically dead shell, with the thickness of d = 1.53 ± 0.3 nm and M_{so} = 50.9 ± 6 emu g^{-1}, in very good agreement with the bulk M_s of Ni (55 emu g^{-1}), confirming the coherence of core−shell model.

The validity of this model is further confirmed by plotting $M_s^{1/3}$ as a function of D^{-1} (Figure 5b). The results are surprisingly consistent, indicating almost constant thickness of disordered layer in the Ni nanoparticles with diameters between 4.2 and 60 nm.

Interestingly, our specimens (Ni/polysilazane and Ni/SiCNO) do not obey the trend of the other Ni nanoparticles. Using the magnetic dead shell with the thickness of d = 1.53 ± 0.3 nm and the M_s of bulk Ni as 50.9 emu g^{-1}, the core−shell model predicts M_s close to zero for the Ni nanoparticles with the diameters of 3.5 and 3.8 nm, much lower than the experimental values of 9.7 and 7.6 emu g^{-1} for the Ni nanoparticles in the Ni/polysilazane and Ni/SiCNO nanocomposites, respectively.

Table 2. M_s (emu g^{-1}) at 300 K as a function of size (nm) of spherical fcc-Ni nanoparticles[a]

size	M_s	ref
60	40	50
35	48.5	51
21	21	52
16	27	50
13	27.9	53
11	19	53
7	7.9	53
5	2.5	in the Supporting Information of ref 54
4.2	2.1	33
3.8	7.64[c]	Ni/SiCNO
3.5	9.67[b]	Ni/polysilazane

[a] M_s of the Ni nanoparticles in the Ni/polysilazane and Ni/SiCNO nanocomposites are calculated from the fitted M_s (Figure 2b), taking into account the Ni nanoparticles contents in each case. [b] M_s(Ni nanoparticles) = M_s(Ni/polysilazane, 0.60) × 100/6.20 = 9.67 emu g^{-1}. [c] M_s(Ni nanoparticles) = M_s(Ni/SiCNO, 0.68) × 100/8.87 = 7.64 emu g^{-1}.

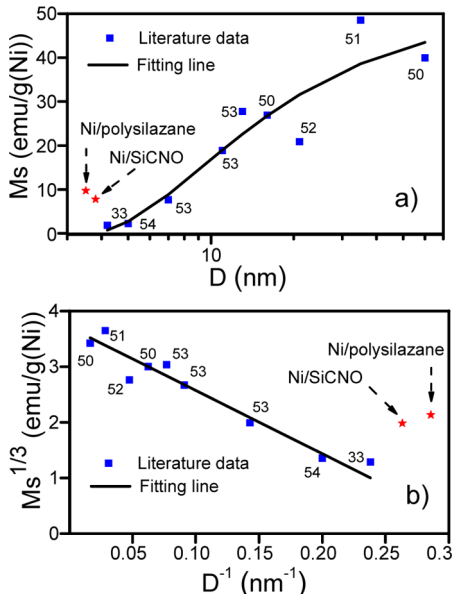

Figure 5. (a) Experimentally measured saturation magnetization, M_s, of spherical fcc-Ni nanoparticles at 300 K as a function of their diameter, D, from the literature (blue square)[33,50−54] fitted by eq 4. Black line, $M_s = 50.8 \times (1-2 \times 1.53/D)^3$, $R^2 = 0.93$. (b) Linearization of the pervious plot, where the constancy of thickness of the magnetically disordered layer, d, as a function of the particles size, D, can be observed, $M_s^{1/3} = 3.70 \times (1-2 \times 1.53 \times D^{-1})$, $R^2 = 0.96$. The Ni/polysilazane and Ni/SiCNO nanocomposites are indicated with red asterisks and are not used in the fitted curves.

As the Ni/polysilazane and Ni/SiCNO nanocomposites show no blocking temperature (Figure 2a), the effect of dipole moments and interactions between the Ni nanoparticles can be completely neglected at 300 K. Therefore, only surface effects are responsible for the anomalous high M_s values in the Ni/polysilazane and Ni/SiCNO nanocomposites.

We assume that the high M_s in the Ni/polysilazane and Ni/SiCNO nanocomposites are because of thinner magnetic dead shell. We explain thinner magnetic dead shell in our specimens, in comparison to that of other Ni nanoparticles, 1.53 ± 0.3 nm, by the stabilizing effect of polymeric and ceramic matrixes.

The lower level of oxygen impurities could play a determining role, i.e. the thinner magnetic dead shell of the Ni nanoparticles in the Ni/polysilazane and Ni/SiCNO nanocomposites could be due to a lower level of oxygen impurities in the shell of Ni nanoparticles. This is easily understood taking into account the synthesis techniques and the microstructure of our specimens. We applied strict Schlenk techniques in an oxygen-free and moisture-free atmosphere throughout the synthesis and characterization of our specimens. Amphiphilic polysilazane molecules protect Ni nanoparticles—in situ generated in polysilazane—against the diffusion of oxygen.

The Ni/SiCNO nanocomposite has higher nickel content and larger Ni nanoparticles compared to the Ni/polysilazane nanocomposite, 8.9 wt % and 3.8 nm in the Ni/SiCNO nanocomposite vs 6.9 wt % and 3 nm the Ni/polysilazane nanocomposite, respectively. However, the M_s of Ni nanoparticles in the Ni/SiCNO nanocomposite is smaller, 7.6 ± 0.09 emu g^{-1}, than that of Ni/polysilazane nanocomposite, 9.7 ± 0.12 emu g^{-1}.

The Ni/SiCNO nanocomposite is produced by the thermolysis of Ni/polysilazane at 700 °C under an Ar atmosphere. During the thermolysis of the Ni/SiCNO nanocomposite, the surfaces of the Ni nanoparticles are affected by oxygen diffusion from the matrix, resulting in a thicker dead shell and a reduction in the M_s of the Ni nanoparticles, compared to those in the Ni/polysilazane nanocomposite. However, we have to note that the thickness of the magnetic dead layer in the Ni nanoparticles of the Ni/SiCNO nanocomposite is still lower than the other reported Ni nanoparticles,[33,50−56] resulting in much higher M_s value in the Ni nanoparticles of the Ni/SiCNO nanocomposite compared to the Ni nanoparticles of comparable size.

In the following section, we show that the Ni/SiCNO nanocomposite can be shaped to prepare a wide variety of structures, including ceramic membranes.

The high M_s value of Ni nanoparticles in Ni/SiCNO nanocomposite indicates that the surfaces of Ni nanoparticles are free of oxide layers, which could bring interesting affinity with gas species such as H_2 during gas separation.

Ni/SiCNO Ceramic Monolith, Foam, and Membrane. Figure 6a displays Ni/SiCNO monolith thermolyzed at 700 °C with 80% yield and 15% contraction compared to the original green body.

Figure 6b shows Ni/SiCNO ceramic foam obtained by a dip coating of polyurethane foam as a sacrificial template into the

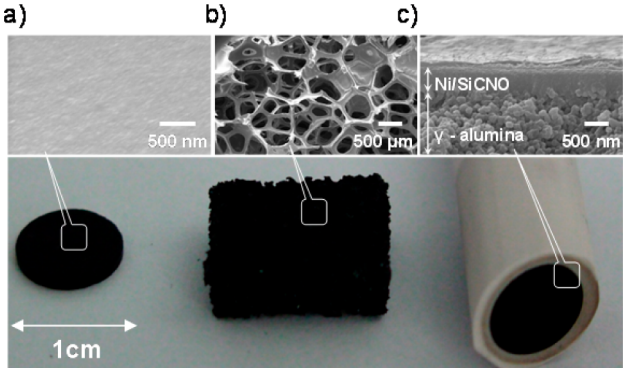

Figure 6. Ni/polysilazane is shaped to make (a) ceramic monolith, (b) ceramic foam, and (c) ceramic membrane.

Ni/polysilazane nanocomposite dispersion in THF followed by thermolysis at 700 °C under an inert atmosphere. The formation of Ni/SiCNO ceramic foam is associated with 72% yield and 20% contraction compared to the original Ni/polysilazane nanocomposite and polyurethane foam template, respectively.

Figure 6c displays a thin Ni/SiCNO membrane obtained by a dip-coating of γ-Al_2O_3 coated tubular substrate into the Ni/polysilazane nanocomposite dispersed in THF followed by thermolysis at 700 °C under an inert atmosphere. The Ni/SiCNO bulk ceramics obtained from the thermolysis of the Ni/polysilazane nanocomposite at 700 °C under an inert atmosphere are nanoporous, revealing a BET surface area of 215 m^2 g^{-1}, a micropore surface area of 205 m^2 g^{-1}, and a micropore volume of 0.113 cm^3 g^{-1}.[29] In the next section we describe the gas permeance characteristics of Ni/SiCNO membrane.

Gas Permeance Characteristics of Ni/SiCNO Membrane. The gas permeance characteristics of the Ni/SiCNO ceramic membrane before and after hydrothermal treatment are summarized in Tables 3 and 4 (extended tables are indicated in Tables S1 and Table S2 in the Supporting Information) and Figure 7.

Table 3. Single Gas Permeance (S.G.P.) before and after Hydrothermal Treatment (H.T.) at 25 and 300 °C for He, H_2, CO_2, C_4H_8, and SF_6

		S.G.P. (× 10^{-7} mol m^{-2} s^{-1} Pa^{-1})				
T (°C)	H.T.	He	H_2	CO_2	C_4H_8	SF_6
25	before	13.56	20.23	5.75	5.82	2.54
25	after	7.53	11.32	2.48	2.79	1.35
300	before	15.10	20.42	3.95	3.28	1.89
300	after	16.62	35.12	5.86	7.09	3.55

Table 4. Hydrogen Permselectivity Characteristics (Ratio of Permeance of H_2 to Permeance of Other Gases) for Ni/SiCNO Ceramic Membrane at 25 and 300 °C before and after Hydrothermal Treatment

T (°C)	H.T.	He	H_2	CO_2	C_4H_8	SF_6
theoretical Knudsen permselectivity (α_{12})						
		1.41	1.0	4.69	5.29	8.54
experimental permselectivity before and after hydrothermal treatment (H.T.) at 25 and 300 °C						
25	before	1.49	1.0	3.52	3.47	8.00
25	after	1.50	1.0	4.56	4.06	8.38
300	before	1.35	1.0	5.17	6.23	10.80
300	after	2.11	1.0	6.00	4.95	9.89

The gas permeance of as-prepared membrane (Figure 7a) before hydrothermal treatment indicates that increase in temperature leads to the decrease in the permeance (P) of gases (except for slight increase in He and H_2 permeance), delineating that the Knudsen diffusion is responsible for the gas transport in the membrane

$$P = \frac{\varepsilon d_p}{\tau L}\left(\frac{8}{9\pi MRT}\right)^{0.5} \quad (5)$$

where ε, d_p, τ, L, R, T and M are the porosity of the membrane, pore diameter, tortuosity, mean membrane thickness, gas constant, absolute temperature and molecular weight of the diffusing gas. The experimental permselectivities are close to those of the theoretical Knudsen values (α_{12}, Table S2 in the Supporting Information), which are inversely proportional to the molecular mass of molecules that are intended to be separated

$$\alpha_{12} = \left(\frac{M_2}{M_1}\right)^{0.5} \quad (6)$$

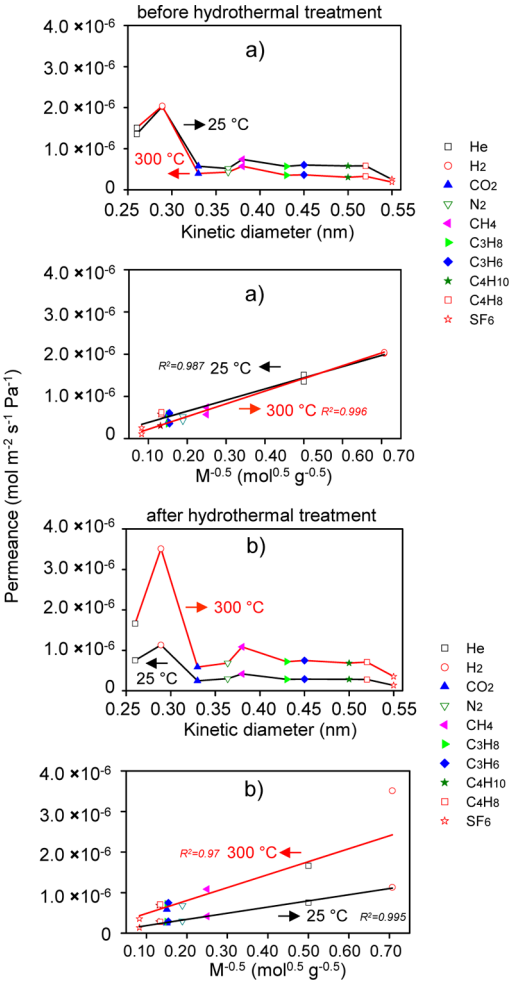

Figure 7. Permeance characteristics of Ni/SiCNO ceramic membrane (a) before and (b) after hydrothermal treatment at 25 and 300 °C.

After the hydrothermal treatment, the temperature dependence of gas permeance is reversed (Figure 7b), i.e., as the temperature increases, the gas permeations increase as well.

To simulate the effects of the hydrothermal treatment, Ni/SiCNO ceramic powder (obtained from the thermolysis of the Ni/polysilazane) is treated under hydrothermal conditions. After the hydrothermal treatment, the Ni/SiCNO ceramic powder has a very low N_2-adsorption, indicating a BET surface area of less than 5 m^2 g^{-1}.

It is noteworthy that before hydrothermal treatment the Ni/SiCNO ceramic powder has a BET surface area of 215 m^2 g^{-1}, a micropore surface area of 205 m^2 g^{-1}, and a micropore volume of 0.113 cm^3 g^{-1} (BET isotherm is shown in Figure S4 in the Supporting Information).[29] The permeance of the membrane after hydrothermal treatment at 300 °C has increased compared to 25 °C. Therefore, the microporous structure of the Ni/SiCNO membrane after hydrothermal treatment contains

dx.doi.org/10.1021/am501892z | ACS Appl. Mater. Interfaces 2014, 6, 12270−12278

micropores that are smaller than those before the hydrothermal treatment.

A typical reaction which is suggested to be responsible for the closure of micropores of microporous silica membranes is the condensation of silanol (Si−OH) bonds.[6] The as-formed Si−OH bonds before or after hydrothermal treatments tend to condense back to siloxane (Si−O−Si) bonds. The Si−OH bonds on the surfaces of the pores follow the thermodynamic principles to reduce the Gibbs free energy on the surfaces of the pores. This could be achieved only by reducing the surface energies, which favor the closure and disappearance of the pores.

The evidence that the formation of Si−OH groups are responsible for the instability of membranes is related to the fact that the microporous silica membranes that are produced at about 600 °C are highly hydrophobic and are more stable than those that are prepared at lower temperatures.[3−6]

The XRD pattern of the Ni/SiCNO ceramic powder after hydrothermal treatment indicates that the Ni nanoparticles are partially reacted and transformed into nickel hydroxide hydrate (Figure S2 in the Supporting Information).

Furthermore, some of the OH- groups of nickel hydroxide hydrate formed on the surface of the Ni nanoparticles during hydrothermal treatment have reacted with the -SiOH bonds of the ceramic matrix, resulting in the formation of Ni−O−Si units. The formation of OH− and Ni−O−Si bonds is confirmed by the FTIR spectrum of the Ni/SiCNO ceramic powder after hydrothermal treatment (see Figure S3 in the Supporting Information), which shows a shoulder at 940−910 cm^{-1} and a broad band at 3700−3100 cm^{-1}, which are ascribed to the presence of Ni−O−Si and OH− bonds, respectively.

The hydrothermal stability of the Ni/SiCNO could be related to the Ni−O−Si bonds, which are interpreted to be responsible for the hydrothermal stability of Ni/SiO_2 membranes as well.[16,17] The formation of Ni−O−Si bonds increases the network density of the matrix leading to the observed hydrothermal stability.

A careful investigation of the results in Table 4 and Figure 7b shows that after the hydrothermal treatment, the permeance of gases is higher as the temperature increases and the H_2 permeance is enhanced even more significantly compared to that of other gases at 300 °C. This finding could be because of the shrinkage of microporous structure of the membrane, providing in situ formed micropore channels with approximately 0.3 nm in size, suitable for the activated diffusion of hydrogen observed for silica membranes.

However, as shown in Table 4 and Figure 7b (after the hydrothermal treatment), at 300 °C, the increase in the permeance of helium (the smallest gas molecule) compared to 25 °C is still apparently lower than that of hydrogen.

Accordingly, the dominant reason for the apparent enhancement in the hydrogen permeance is not only related to the contribution of the activated diffusion. Therefore, as indicated in Table 4 and Figure 7b, the increase in the hydrogen permeance at 300 °C should be considered also selective.

The in situ formed Ni−OH during the hydrothermal treatment are highly reactive, and easily reduced to be nickel species. This is confirmed by the heat treatment of a sample under H_2 (compare Figure S2b and c in the Supporting Information) and is reported for the Ni/SiO_2 membranes as well.[16]

In other words, a reason for the more pronounced enhancement in the hydrogen permeance at 300 °C compared to that of 25 °C after hydrothermal treatment could be related to the well-known hydrogen affinity of the metal nickel.[57−59]

In summary, after the hydrothermal treatment the large micropores in the ceramic matrix collapse and the shrinkage of the microporous structure of ceramic matrix occurs, whereas some defects and large pores are retained. Therefore, the Knudsen diffusion through the defects and large micropores becomes influenced by the effect of activated diffusion because of the in situ formed micropore channels, with the opportunity for the additional selective mechanism for the transport of H_2 molecules because of their affinity with the surfaces of Ni nanoparticles.

Outlook for Design of Catalytic Membrane Reactors. Here, we describe the potential of developed synthesis and shaping techniques for the construction of catalytic membrane reactors. The catalytic hydrogenation of carbon dioxide to methane (Sabatier reaction) is an important catalytic reaction.[60]

Highly dispersed Ni nanoparticles on supports have shown high potential for Sabatier reaction.[60] Our synthesis strategy is potentially applicable for the design of catalytic membrane reactors and could meet the requirements involved in their design.

We have demonstrated in the current work that (i) different shapes of Ni/SiCNO ceramic can be fabricated, (ii) high permeances through ceramic membranes are obtained, (iii) Ni nanoparticles show affinity with respect to hydrogen and they stabilize the structure under hydrothermal conditions.

The fabrication of a tubular porous ceramic reactor from Ni/SiCNO material is possible, which could be combined with a selective microporous ceramic layer. This membrane and catalyst composite could reduce the scale and increase the productivity of a potential membrane reactor.

CONCLUSIONS

The Ni nanoparticles are in situ formed at room temperature in a reaction between the Ni(II)-complex and the commercial polysilazane HTT. Electron transfer from negatively charged hydrogen in the silane group ($Si^{+\delta}$-$H^{-\delta}$) to the Ni^{2+} in the Ni(II)-complex induces the Ni^{2+} reduction with simultaneous nucleophilic substitution of ethanolamine at the Si centers, which leads to the formation of aminoethoxysilyl groups ($NH_2CH_2CH_2OSi$-) and acetoxysilyl (CH_3COOSi-) groups. As a result, the Ni nanoparticles become in situ stabilized by the amphiphilic polysilazane molecules, protecting them against agglomeration and growth.

After the thermolysis of the Ni/polysilazane nanocomposite at 700 °C under an Ar atmosphere, the average size and superparamagnetism of Ni nanoparticles are preserved in the Ni/SiCNO nanocomposite, indicating a higher than expected saturation magnetization as well.

The Ni/polysilazane nanocomposite (solution) can be shaped to prepare a variety of ceramics, including ceramic monolith, foam and membrane. The gas separation performance of synthesized membranes shows that the presence of Ni nanoparticles is effective to prepare hydrothermally stable membranes.

Our synthesis and design strategy is well-extendable to other transition metals allowing for the synthesis of metal/polysilazane and metal/ceramic nanocomposites. Potential candidates are Fe, Co, and Cu; this work is now on going.

■ ASSOCIATED CONTENT

Supporting Information

Table S1 and Table S2: Single gas permeance and hydrogen permselectivity characteristics of membrane. Figure S1: TEM and HRTEM micrographs of Ni/polysilazane and Ni/SiCNO nanocomposites. Figures S2 and S3: XRD and FTIR of specimens before and after hydrothermal and hydrogen treatments. Figure S4: BET isotherm of Ni/SiCNO powder before hydrothermal treatment. Comparison of gas separation performance of Ni/SiCNO with Ni/SiO_2 membranes (from literature). This material is available free of charge via the Internet at http://pubs.acs.org.

■ AUTHOR INFORMATION

Corresponding Author

*E-mail: mahdi.seifollahi.bazarjani@uni-oldenburg.de.

Present Addresses

‡M.S.B. is currently at Carl von Ossietzky Universität Oldenburg, Institute für Chemie, Carl von Ossietzky Strasse 9−11, D-26129 Oldenburg, Germany

#A.G. is currently at Technische Universität Berlin, Institut für Werkstoffwissenschaften und -technologien, Fachgebiet Keramische Werkstoffe, Hardenbergstrasse 40, D-10623 Berlin, Germany

Author Contributions

The manuscript was written through contributions of all authors. All authors have given approval to the final version of the manuscript.

Notes

The authors declare no competing financial interest.

■ ACKNOWLEDGMENTS

This work was performed within the framework of the project "Thermoresistant ceramic membrane with integrated gas sensor for high temperature separation and detection of hydrogen and carbon monoxide" of the priority program "Adapting surfaces for high temperature applications" (DFG-SPP 1299, www.spp-haut.de, DFG - German Research Foundation). R.R. thanks the Fonds der Chemischen Industrie, Frankfurt, Germany, for continuous financial support.

■ REFERENCES

(1) Tsuru, T. Development of Metal-Doped Silica Membranes for Increased Hydrothermal Stability and Their Applications to Membrane Reactors for Steam Reforming of Methane. *J. Jpn. Pet. Inst.* **2011**, *54*, 277−286.

(2) Igi, R.; Yoshioka, T.; Ikuhara, Y. H.; Iwamoto, Y.; Tsuru, T. Characterization of Co-Doped Silica for Improved Hydrothermal Stability and Application to Hydrogen Separation Membranes at High Temperatures. *J. Am. Ceram. Soc.* **2008**, *91*, 2975−2981.

(3) Seshimo, M.; Saito, T.; Akamatsu, K.; Segawa, A.; Nakao, S. Influence of Toluene Vapor on the H_2-Selective Performance of Dimethoxydiphenylsilane-Derived Silica Membranes Prepared by the Chemical Vapor Deposition Method. *J. Membr. Sci.* **2012**, *415*, 51−56.

(4) Akamatsu, K.; Nakane, M.; Sugawara, T.; Nakao, S. Performance under Thermal and Hydrothermal Condition of Amorphous Silica Membrane Prepared by Chemical Vapor Deposition. *AIChE J.* **2009**, *55*, 2197−2200.

(5) Ohta, Y.; Akamatsu, K.; Sugawara, T.; Nakao, A.; Miyoshi, A.; Nakao, S. Development of Pore Size-Controlled Silica Membranes for Gas Separation by Chemical Vapor Deposition. *J. Membr. Sci.* **2008**, *315*, 93−99.

(6) Nomura, M.; Seshimo, M.; Aida, H.; Nakatani, K.; Gopalakrishnan, S.; Sugawara, T.; Ishikawa, T.; Kawamura, M.; Nakao, S. Preparation of a Catalyst Composite Silica Membrane Reactor for Steam Reforming Reaction by using a Counter Diffusion CVD Method. *Ind. Eng. Chem. Res.* **2006**, *45*, 3950−3954.

(7) de Vos, R. M.; Verweij, H. High-Selectivity, High-Flux Silica Membranes for Gas Separation. *Science* **1998**, *279*, 1710−1711.

(8) Bazarjani, M. S.; Hojamberdiev, M.; Morita, K.; Zhu, G. Q.; Cherkashinin, G.; Fasel, C.; Herrmann, T.; Breitzke, H.; Gurlo, A.; Riedel, R. Visible Light Photocatalysis with c-WO_{3-x}/WO_3×H_2O Nanoheterostructures *In situ* Formed in Mesoporous Polycarbosilane-Siloxane Polymer. *J. Am. Chem. Soc.* **2013**, *135*, 4467−4475.

(9) Hojamberdiev, M.; Prasad, R. M.; Morita, K.; Zhu, Y. F.; Schiavon, M. A.; Gurlo, A.; Riedel, R. Template-Free Synthesis of Polymer-Derived Mesoporous SiOC/TiO_2 and SiOC/N-Doped TiO_2 Ceramic Composites for Application in the Removal of Organic Dyes from Contaminated Water. *Appl. Catal., B* **2012**, *115*, 303−313.

(10) Hojamberdiev, M.; Prasad, R. M.; Morita, K.; Schiavon, M. A.; Riedel, R. Polymer-Derived Mesoporous SiOC/ZnO Nanocomposite for the Purification of Water Contaminated with Organic Dyes. *Microporous Mesoporous Mater.* **2012**, *151*, 330−338.

(11) Graczyk-Zajac, M.; Fasel, C.; Riedel, R. Polymer-Derived-SiCN Ceramic/Graphite Composite as Anode Material with Enhanced Rate Capability for Lithium Ion Batteries. *J. Power Sources* **2011**, *196*, 6412−6418.

(12) Prasad, R. M.; Iwamoto, Y.; Riedel, R.; Gurlo, A. Multilayer Amorphous-Si-B-C-N/γ-Al_2O_3/α-Al_2O_3 Membranes for Hydrogen Purification. *Adv. Eng. Mater.* **2010**, *12*, 522−528.

(13) Seifollahi Bazarjani, M.; Müller, M.; Kleebe, H.-J.; Fasel, C.; Gurlo, A.; Riedel, R. In situ Formation of Tungsten Oxycarbide, Tungsten Carbide and Tungsten Nitride Nanoparticles in Micro- and Mesoporous Polymer-Derived Ceramics. *J. Mater. Chem. A* **2014**, *2*, 10454−10464.

(14) Elyassi, B.; Sahimi, M.; Tsotsis, T. T. A Novel Sacrificial Interlayer-Based Method for the Preparation of Silicon Carbide Membranes. *J. Membr. Sci.* **2008**, *316*, 73−79.

(15) Elyassi, B.; Sahimi, M.; Tsotsis, T. T. Silicon Carbide Membranes for Gas Separation Applications. *J. Membr. Sci.* **2007**, *288*, 290−297.

(16) Ikuhara, Y. H.; Mori, H.; Saito, T.; Iwamoto, Y. High-Temperature Hydrogen Adsorption Properties of Precursor-Derived Nickel Nanoparticle-Dispersed Amorphous Silica. *J. Am. Ceram. Soc.* **2007**, *90*, 546−552.

(17) Yamazaki, S.; Uno, N.; Mori, H.; Ikuhara, Y. H.; Iwamoto, Y.; Kato, T.; Hirayama, T. TEM Observation of Hydrogen Permeable Si-M-O (M = Ni or Sc) Membranes Synthesized on Mesoporous Anodic Alumina Capillary Tubes. *J. Mater. Sci.* **2006**, *41*, 2679−2683.

(18) Yoshida, K.; Ikuhara, Y. H.; Takahashi, S.; Hirayama, T.; Saito, T.; Sueda, S.; Tanaka, N.; Gai, P. L. The Three-Dimensional Morphology of Nickel Nanodots in Amorphous Silica and their Role in High-Temperature Permselectivity for Hydrogen Separation. *Nanotechnol.* **2009**, *20*, 315703−315711.

(19) Gu, Y. F.; Oyama, S. T. Permeation Properties and Hydrothermal Stability of Silica-Titanic Membranes Supported on Porous Alumina Substrates. *J. Membr. Sci.* **2009**, *345*, 267−275.

(20) Boffa, V.; Castricum, H. L.; Garcia, R.; Schmuhl, R.; Petukhov, A. V.; Blank, D. H. A.; ten Elshof, J. E. Structure and Growth of Polymeric Niobia-Silica Mixed-Oxide Sols for Microporous Molecular Sieving Membranes: A SAXS Study. *Chem. Mater.* **2009**, *21*, 1822−1828.

(21) Boffa, V.; ten Elshof, J. E.; Petukhov, A. V.; Blank, D. H. A. Microporous Niobia-Silica Membrane with Very Low CO_2 Permeability. *ChemSusChem* **2008**, *1*, 437−443.

(22) Ionescu, E.; Kleebe, H. J.; Riedel, R. Silicon-Containing Polymer-Derived Ceramic Nanocomposites (PDC-NCs): Preparative Approaches and Properties. *Chem. Soc. Rev.* **2012**, *41*, 5032−5052.

(23) Zaheer, M.; Schmalz, T.; Motz, G.; Kempe, R. Polymer-Derived non-Oxide Ceramics Modified with Late Transition Metals. *Chem. Soc. Rev.* **2012**, *41*, 5102−5116.

(24) Bala, T.; Gunning, R. D.; Venkatesan, M.; Godsell, J. F.; Roy, S.; Ryan, K. M. Block Copolymer Mediated Stabilization of Sub-5 nm

Superparamagnetic Nickel Nanoparticles in an Aqueous Medium. *Nanotechnol.* **2009**, *20*, 415603−415613.
(25) Behrens, S. Preparation of Functional Magnetic Nanocomposites and Hybrid Materials: Recent Progress and Future Directions. *Nanoscale* **2011**, *3*, 877−892.
(26) Jia, C. J.; Schuth, F. Colloidal Metal Nanoparticles as a Component of Designed Catalyst. *Phys. Chem. Chem. Phys.* **2011**, *13*, 2457−2487.
(27) Bockstaller, M. R.; Mickiewicz, R. A.; Thomas, E. L. Block Copolymer Nanocomposites: Perspectives for Tailored Functional Materials. *Adv. Mater.* **2005**, *17*, 1331−1349.
(28) Lu, A. H.; Salabas, E. L.; Schuth, F. Magnetic Nanoparticles: Synthesis, Protection, Functionalization, and Application. *Angew. Chem., Int. Ed.* **2007**, *46*, 1222−1244.
(29) Bazarjani, M. S.; Kleebe, H. J.; Müller, M. M.; Fasel, C.; Baghaie Yazdi, M.; Gurlo, A.; Riedel, R. Nanoporous Silicon Oxycarbonitride Ceramics Derived from Polysilazanes In situ Modified with Nickel Nanoparticles. *Chem. Mater.* **2011**, *23*, 4112−4123.
(30) Bazarjani, M. S.; Foro, S.; Donner, W.; Gurlo, A.; Riedel, R. Trans-bis(acetato-*k*O)bis(2-aminoethanol-k^2N,O)nickel(II). *Acta Cryst. E* **2012**, *23*, m567−m568.
(31) Jüttke, Y.; Richter, H.; Voigt, I.; Prasad, R. M.; Bazarjani, M. S.; Gurlo, A.; Riedel, R. Polymer-Derived Ceramic Membranes for Gas Separation. *Chem. Eng. Trans.* **2013**, *32*, 1891−1896.
(32) Yulikov, M. M.; Purtov, P. A. FMR Study of Superparamagnetic Ni Particles with Weak and Strong Magnetic Anisotropy. *Appl. Magn. Reson.* **2005**, *29*, 231−249.
(33) Ramirez-Meneses, E.; Betancourt, I.; Morales, F.; Montiel-Palma, V.; Villanueva-Alvarado, C. C.; Hernandez-Rojas, M. E. Superparamagnetic Nickel Nanoparticles Obtained by an Organometallic Approach. *J. Nanopart. Res.* **2011**, *13*, 365−374.
(34) Yoon, M.; Kim, Y.; Kim, Y. M.; Volkov, V.; Song, H. J.; Park, Y. J.; Park, I. W. Superparamagnetic Properties of Nickel Nanoparticles in an Ion-Exchange Polymer Film. *Mater. Chem. Phys.* **2005**, *91*, 104−107.
(35) Roy, A.; Srinivas, V.; Ram, S.; De Toro, J. A.; Riveiro, J. M. Effect of Interstitial Oxygen on the Crystal Structure and Magnetic Properties of Ni Nanoparticles. *J. Appl. Phys.* **2004**, *96*, 6782−6788.
(36) Khanna, S. N.; Linderoth, S. Magnetic-Behavior of Clusters of Ferromagnetic Transition-Metals. *Phys. Rev. Lett.* **1991**, *67*, 742−745.
(37) Chen, Q.; Zhang, Z. J. Size-Dependent Superparamagnetic Properties of $MgFe_2O_4$ Spinel Ferrite Nanocrystallites. *Appl. Phys. Lett.* **1998**, *73*, 3156−3158.
(38) LesliePelecky, D. L.; Rieke, R. D. Magnetic Properties of Nanostructured Materials. *Chem. Mater.* **1996**, *8*, 1770−1783.
(39) Billas, I. M. L.; Chatelain, A.; Deheer, W. A. Magnetism from the Atom to the Bulk in Iron, Cobalt, and Nickel Clusters. *Science* **1994**, *265*, 1682−1684.
(40) de Montferrand, C.; Lalatonne, Y.; Bonnin, D.; Lievre, N.; Lecouvey, M.; Monod, P.; Russier, V.; Motte, L. Size-Dependent Nonlinear Weak-Field Magnetic Behavior of Maghemite Nanoparticles. *Small* **2012**, *8*, 1945−1956.
(41) Millan, A.; Urtizberea, A.; Silva, N. J. O.; Palacio, F.; Amaral, V. S.; Snoeck, E.; Serin, V. Surface Effects in Maghemite Nanoparticles. *J. Magn. Magn. Mater.* **2007**, *312*, L5−L9.
(42) De Biasi, E.; Ramos, C. A.; Zysler, R. D.; Romero, H. Large Surface Magnetic Contribution in Amorphous Ferromagnetic Nanoparticles. *Phys. Rev. B* **2002**, *65*, 144416.
(43) De Biasi, E.; Zysler, R. D.; Ramos, C. A.; Romero, H.; Fiorani, D. Surface Anisotropy and Surface-Core Interaction in Co-Ni-B and Fe-Ni-B Dispersed Amorphous Nanoparticles. *Phys. Rev. B* **2005**, *71*.
(44) Gangopadhyay, S.; Hadjipanayis, G. C.; Dale, B.; Sorensen, C. M.; Klabunde, K. J.; Papaefthymiou, V.; Kostikas, A. Magnetic-Properties of Ultrafine Iron Particles. *Phys. Rev. B* **1992**, *45*, 9778−9787.
(45) Knobel, M.; Nunes, W. C.; Socolovsky, L. M.; De Biasi, E.; Vargas, J. M.; Denardin, J. C. Superparamagnetism and other Magnetic Features in Granular Materials: A Review on Ideal and Real Systems. *J. Nanosci. Nanotechnol.* **2008**, *8*, 2836−2857.
(46) Singh, V.; Srinivas, V.; Ranot, M.; Angappane, S.; Park, J. G. Effect of Polymer Coating on the Magnetic Properties of Oxygen-Stabilized Nickel Nanoparticles. *Phys. Rev. B* **2010**, *82*.
(47) Tronc, E.; Ezzir, A.; Cherkaoui, R.; Chaneac, C.; Nogues, M.; Kachkachi, H.; Fiorani, D.; Testa, A. M.; Greneche, J. M.; Jolivet, J. P. Surface-Related Properties of γ-Fe_2O_3 Nanoparticles. *J. Magn. Magn. Mater.* **2000**, *221*, 63−79.
(48) Vasilakaki, M.; Trohidou, K. N. Surface Effects on the Magnetic Behaviour of Nanoparticles with Core/Shell Morphology. *J. Phys. D Appl. Phys.* **2008**, *41*.
(49) Issa, B.; Obaidat, I. M.; Albiss, B. A.; Haik, Y. Magnetic Nanoparticles: Surface Effects and Properties Related to Biomedicine Applications. *Int. J. Mol. Sci.* **2013**, *14*, 21266−21305.
(50) Luo, X. H.; Chen, Y. Z.; Yue, G. H.; Peng, D. L.; Luo, X. T. Preparation of Hexagonal Close-Packed Nickel Nanoparticles *via* a Thermal Decomposition Approach using Nickel Acetate Tetrahydrate as a Precursor. *J. Alloys Compd.* **2009**, *476*, 864−868.
(51) Chen, Y. Z.; Peng, D. L.; Lin, D. P.; Luo, X. H. Preparation and Magnetic Properties of Nickel Nanoparticles *via* the Thermal Decomposition of Nickel Organometallic Precursor in Alkylamines. *Nanotechnol.* **2007**, *18*.
(52) Carenco, S.; Boissiere, C.; Nicole, L.; Sanchez, C.; Le Floch, P.; Mezailles, N. Controlled Design of Size-Tunable Monodisperse Nickel Nanoparticles. *Chem. Mater.* **2010**, *22*, 1340−1349.
(53) Wang, H. Y.; Jiao, X. L.; Chen, D. R. Monodispersed Nickel Nanoparticles with Tunable Phase and Size: Synthesis, Characterization, and Magnetic Properties. *J. Phys. Chem. C* **2008**, *112*, 18793−18797.
(54) LaGrow, A. P.; Ingham, B.; Cheong, S.; Williams, G. V. M; Dotzler, C.; Toney, M. F.; Jefferson, D. A.; Corbos, E. C.; Bishop, P. T.; Cookson, J.; Tilley, R. D. Synthesis, Alignment, and Magnetic Properties of Monodisperse Nickel Nanocubes. *J. Am. Chem. Soc.* **2012**, *134*, 855−858.
(55) Bala, T.; Gunning, R. D.; Venkatesan, M.; Godsell, J. F.; Roy, S.; Ryan, K. M. Block copolymer mediated stabilization of sub-5 nm superparamagnetic nickel nanoparticles in an aqueous medium. *Nanotechnology* **2009**, *20*.
(56) Rider, D. A.; Liu, K.; Eloi, J. C.; Vanderark, L.; Yang, L.; Wang, J. Y.; Grozea, D.; Lu, Z. H.; Russell, T. P.; Manners, I. Nanostructured Magnetic Thin Films from Organometallic Block Copolymers: Pyrolysis of Self-Assembled Polystyrene-Block-Poly(ferrocenylethylmethylsilane). *ACS Nano* **2008**, *2*, 263−270.
(57) Chen, Y. Z.; Cui, P.; Xiong, G. X.; Xu, H. Y. Novel Nickel-Based Catalyst for Low Temperature Hydrogen Production from Methane Steam Reforming in Membrane Reformer. *Asia-Pac. J. Chem. Eng.* **2010**, *5*, 93−100.
(58) Ryi, S. K.; Park, J. S.; Kim, D. K.; Kim, T. H.; Kim, S. H. Methane Steam Reforming with a Novel Catalytic Nickel Membrane for Effective Hydrogen Production. *J. Membr. Sci.* **2009**, *339*, 189−194.
(59) Ernst, B.; Haag, S.; Burgard, M. Permselectivity of a Nickel/Ceramic Composite Membrane at Elevated Temperatures: A New Prospect in Hydrogen Separation ? *J. Membr. Sci.* **2007**, *288*, 208−217.
(60) Wang, W.; Wang, S. P.; Ma, X. B.; Gong, J. L. Recent advances in catalytic hydrogenation of carbon dioxide. *Chem. Soc. Rev.* **2011**, *40*, 3703−3727.